Ceramics International 49 (2023) 29755–29767

Contents lists available at ScienceDirect

Ceramics International

journal homepage: www.elsevier.com/locate/ceramint

The implementation of dual-band electromagnetically induced transparency metastructure based on micro-strip line structure and Calcium-magnesium-titanium ceramic

Haining Ye, Baofei Wan, Hanqing Dong, Haifeng Zhang *

College of Electronic and Optical Engineering & College of Flexible Electronics (Future Technology), Nanjing University of Posts and Telecommunications, Nanjing, 210023, China

ARTICLE INFO

Handling Editor: Dr P. Vincenzini

Keywords:
Calcium-magnesium-titanium ceramic
Electromagnetically induced transparency
Micro-strip line

ABSTRACT

In this paper, a metastructure based on micro-strip lines (MSL) structure and Calcium-magnesium-titanium (CMT) is proposed to realize the electromagnetically induced transparency (EIT) phenomenon. In this structure, the MSL as the main structure acts as the bright mode, while the ceramic structure composed of CMT material cylinders acts as the dark mode. The EIT characteristics are simulated and analyzed, while the equivalent circuit model is established. What's more, the EIT effect of the designed structure is verified by experiments, providing convincing evidence for the dual-band EIT performance of the structure. The results show that the dual-band EIT effect is achieved in 0.2 GHz~1.6 GHz by coupling the CMT structure with the MSL structure, and the values of both transmission peaks reach more than 90%. The physical mechanism of the EIT phenomenon is analyzed by simulating the response of bright mode and dark mode to electromagnetic waves, respectively. Compared with the previously studied EIT MSs, the proposed structure can achieve the EIT effect in dual bands with wider bandwidth, which has a certain application value in the field of optical cache.

1. Introduction

The electromagnetically induced transparency (EIT) effect is a quantum destructive interference phenomenon in the atomic system, making an opaque medium transparent and almost zero absorption of light in a medium [1]. The high-intensity dispersion and sharp change of refractive index caused by the EIT effect can be effectively applied in optical cache devices and refractive index sensing, group delay, and so on [2–4]. The EIT effect was first observed by Booller et al. in strontium (Sr) atomic vapors at ultra-low temperatures [5]. At the resonant absorption frequency of the medium, due to the interference effect of the strongly coupled beam, the original single transition level splits into two. When the probe light is incident, a sharp transmission peak is generated at the original level. However, the general EIT effect requires an ultra-stable laser, ultra-low temperature environment, and complex experimental system structure, which limits its further development and application [6,7]. In recent years, many classical means have been proposed for the simulation and implementation of the EIT effect, such as photonic crystals (PCs) [8–11], metastructure (MS) [12], and so on. MS is a kind of artificial structure formed by composite processing, whose units are usually periodically distributed, which can lead to resonant coupling responses with electromagnetic waves (EMW) of different frequency bands [13]. When the EIT effect is realized by MSs, the periodic unit usually consists of at least two kinds of structures: the bright mode which can produce strong resonance with EMW, and the dark mode structure which has a relatively weak response to EMW. If the EMW strikes this type of MS, the bright and dark mode structure will be electromagnetically coupled, and an obvious transmission peak can be formed at the resonant frequency, thus achieving the EIT effect [14]. Besides, MSs can achieve many properties that natural electromagnetic materials do not have, leading to the result that the simulation and implementation of the EIT effect in the MS have attracted great attention from the scientific community due to its advantages such as flexible adjustability, multiple operating bands, large working bandwidth and so on [15–19]. In 2022, a reconfigurable EIT MS using vanadium dioxide material is proposed by Jiang et al., which can achieve absorber and the EIT phenomenon in two states respectively, showing strong tunability [20]. The narrow-band EIT effect in the microwave band is confirmed by Zhu et al. in 2012, which is achieved by coupling three rectangular metal strips to each other [21]. It is reported by Ning et al. that not only

* Corresponding author.
E-mail addresses: hanlor@163.com, hanlor@njupt.edu.cn (H. Zhang).

https://doi.org/10.1016/j.ceramint.2023.06.227
Received 3 May 2023; Received in revised form 17 June 2023; Accepted 21 June 2023
Available online 1 July 2023

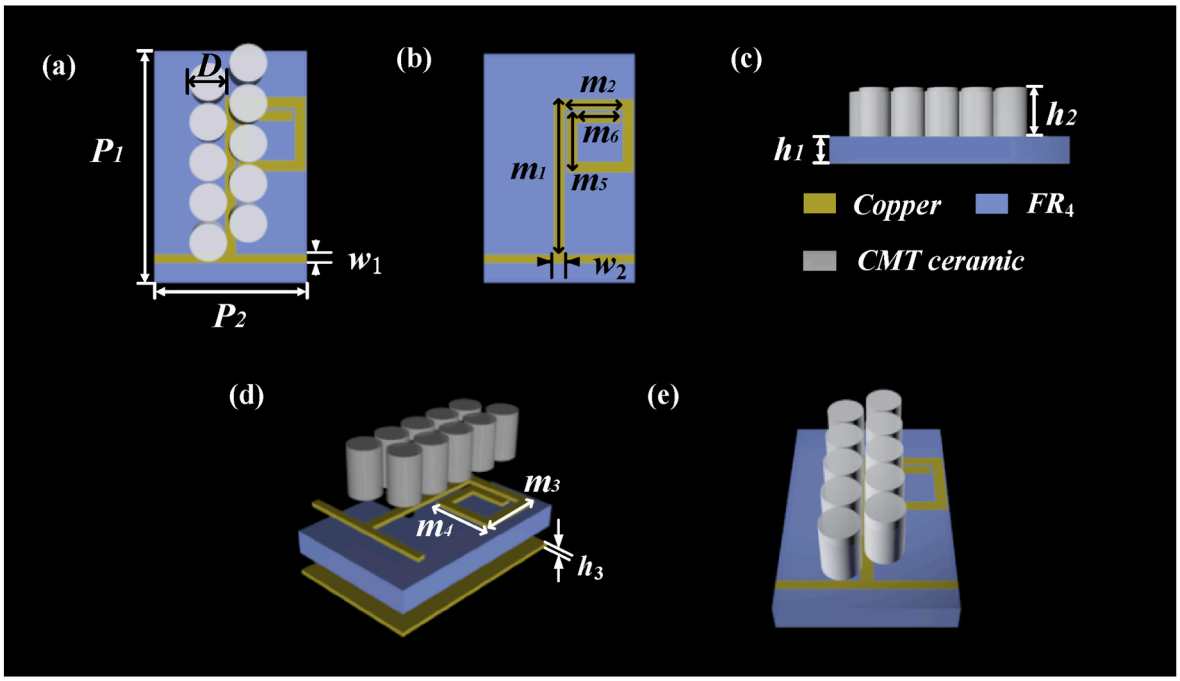

Fig. 1. Schematic views of the model:(a) the top view, (b) the bottom diagram, (c) the side view, (d) the stereoscopic view, and (e) the stereoscopic of the unit cell from the front view.

can the composite structure of graphene MS composed of graphene strip and Lithium fluoride plate produce multi-frequency band EIT effects, but also the obtained transparent windows are broadband [22]. Most of the above studies on EIT MS have adopted planar structures. However, in fact, the three-dimensional structure has the advantages of multi-electromagnetic coupling and multi-dimensional adjustment, which makes it easier to realize multi-band broadband EIT than the planar structure.

Micro-strip line (MSL) is a microwave transmission line composed of a single conductor band supported on a dielectric substrate, with the superiority of easy integration with other microwave devices [23]. When MSL structure is utilized to realize the EIT effect, it is usually used as the bright mode, that is, the mode that has a strong resonance with EMW. On this basis, it is necessary to introduce another dark mode structure with a weaker response with EMW, leading to the result that the bright mode and dark mode are coupled to achieve the EIT effect [24–26].

In the previous works in terms of EIT, few studies involve ceramic materials, but in fact, ceramic materials have many advantages [27–30]. For example, ceramic materials, contrasting with other dielectric material, possesses the merit of thermal stability, low processing cost, and so on [31–35]. Among them, Calcium-magnesium-titanium (known as CMT) microwave dielectric ceramics material is mainly used as an outer ring and gyromagnetic ferrite matching co-sintering, suitable for circulator and isolator at microwave frequency (300 MHz~300 GHz), with its high stability, high dielectric constant, and low loss characteristics. Therefore, the proper utilization of CMT can expand bandwidth, and alleviate the problem of device inter-modulation, which is the reason that CMT is commonly used in microwave filters and oscillators.

In the paper, a dual-band broadband EIT MS is proposed by coupling the MSL structure as bright mode and an all-dielectric structure made of CMT ceramic material as dark mode, which rarely appears simultaneously in previous work. Different from the general multi-mode coupling of multi-band EIT, such as bright-bright-dark or bright-dark-dark coupling, this work only involves the coupling of one bright mode and one dark mode. According to the Four-Level-Tripod (FLT) theory, the principle of EIT can be analyzed. Moreover, the feasibility and rationality of the structure can be verified by circuit fitting and experimental measurement. Finally, by discussing the key parameters of the structure and simulating the electric field distribution, the physical mechanism of the structure is discussed deeply. In terms of use, the proposed dual-band EIT structure has the potential for applications of slow light devices, electromagnetic filters, and MS absorbers.

Table 1
The summary of parameters of the EIT MS.

Parameter	Value(mm)	Parameter	Value(mm)
P_1	53	w_2	2.5
P_2	35	m_1	20
D	7	m_2	13.5
h_1	2	m_3	17
h_2	10	m_4	15.5
h_3	0.035	m_5	14
w_1	2	m_6	10

2. Model design and principle analyze

Fig. 1 shows the schematic diagram of the proposed EIT MS. As shown in Fig. 1, the structure is mainly composed of three parts, namely a combination of a main MSL structure with a quarter-wavelength micro-strip open branch line, a square spiral patch structure, and a group of dielectric cylinders. The material of the dielectric substrate is FR4, whose relative dielectric constant ε_r is 4.4, with a thickness h_1 of 2 mm and a loss angle tangent of 0.02 [36]. A MSL is loaded above the substrate, and a quarter-wavelength micro-strip open-circuit branch line is added to the middle of the MSL, with the square spiral patch on the left

Table 2
The detailed parameters of CMT.

Dielectric constant	40
Quality factor (Qf)	60000
Frequency temperature coefficient (ρpm/°C)	0 ± 3
Frequency range (GHz)	0.3–300

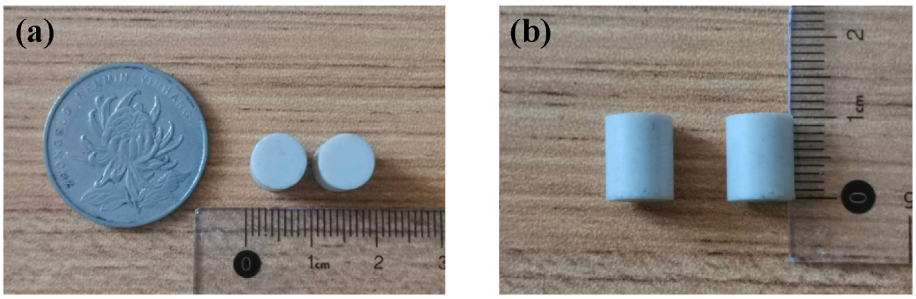

Fig. 2. The physical picture of CMT cylinder: (a) the top view, and (b) the side view.

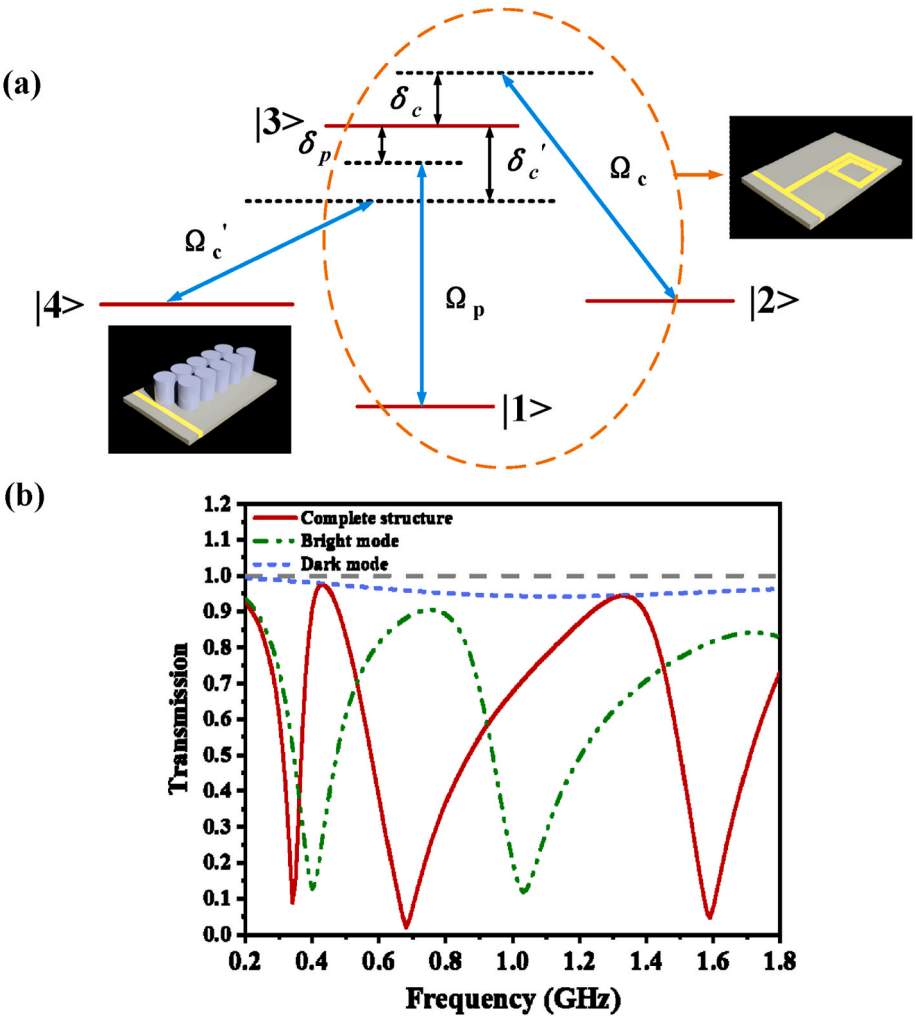

Fig. 3. EIT three-level system: (a) FLT atomic system, and (b) EIT transmission effect.

to realize the bright mode. MSL structure, spiral patch, and metal plate are made of copper with finite conductivity of 5.8×10^7 S/m and the thickness is 0.035 mm [37]. Other specific structural parameters are given in detail in Table 1. A group of ten dielectric cylinders with diameter $\boldsymbol{D}$ is distributed above the quarter branch line of the MSL, made of CMT, with dielectric constant $\boldsymbol{\varepsilon}$ of 40 and relative permeability $\boldsymbol{\mu}$ of 1). The detailed parameters are shown in Table 2 and the specific appearance of the CMT ceramic body is shown in Fig. 2.

The dual-band EIT effect usually occurs in the FLT system of atoms [38]. The conceptual diagram of energy levels is shown in Fig. 3(a). In the process of energy level transition, the transition between |1> and |3> is driven by the probe light, whose frequency is the Rabi frequency Ω_p. As for the transition between |2> and |3>, the coupling light with the Rabi frequency Ω_c plays a role in exciting the transition. These two different excitation paths interfere destructively, making the initially opaque medium transparent. Among them, energy levels |1>, |2>, and |3> form a three-level system together, leading to the single band EIT. When another state |4> is introduced, the three-level system will turn into a FLT system. Attributed to the change from destructive interference to constructive interference, which is produced between the three-level system and control state |4>, a new transmission peak will be generated in the structure to achieve a dual-band EIT effect. In this structure, the MSL structure acts as a three-level system, demonstrating an EIT-like phenomenon. With the CMT structure introduced, it couples

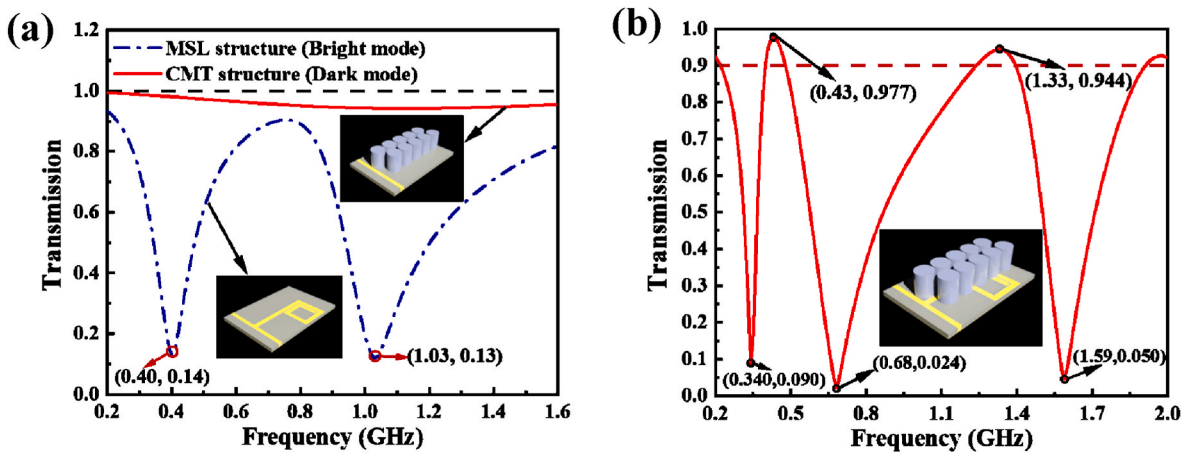

Fig. 4. Transmission spectra:(a) transmission of bright mode and dark mode, and (b) transmission of complete structure.

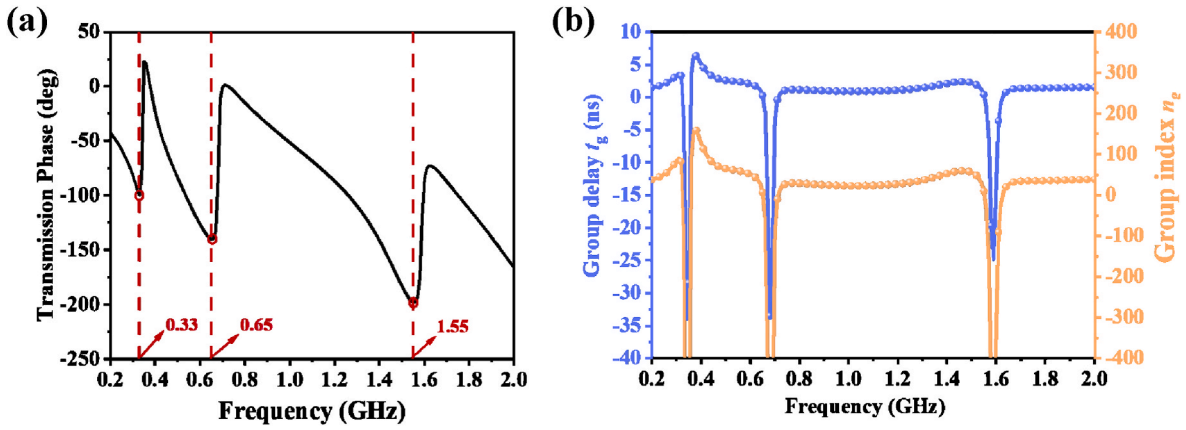

Fig. 5. The curves of transmission phase, group delay and group index:(a) transmission phase, and (b) group delay and group index.

with the MSL structure, bringing about dual-band EIT based on the single-band EIT.

3. Simulation and experiment

The electromagnetic response of bright and dark modes acting separately is simulated respectively in High Frequency Structure Simulator (HFSS), giving rise to the results in Fig. 4(a). When the two modes work together, the EIT effect can be produced as shown in Fig. 4(b). Spiral wire structure with MSL responds strongly to EMW, which is the reason that it plays a role as the bright mode of the proposed EIT MS. The MSL structure resonates strongly with the EMW at 1.03 GHz, resulting in a trough with a transmittance of 0.13. At 0.4 GHz, the MSL structure couples with the spiral wire structure to form another transmission dip with a value of 0.14. As for CMT structure, a slight resonance is generated by coupling it with EMW, for which it is defined as dark mode. Integrating bright mode with dark mode, a new transmission peak will be generated in the frequency band that is not originally transmitted due to destructive interference, which is considered the EIT effect. As can be seen from Fig. 4(b), the proposed EIT MS forms two transparent windows, respectively 0.34 GHz~0.68 GHz and 0.68 GHz~1.59 GHz. In Fig. 4(b), there are two new transmission peaks at 0.43 GHz and 1.33 GHz respectively in the complete structure, which are not transmission points when the bright mode or dark mode acts alone.

When the EIT effect occurs, the transmission phase in the transparent window changes dramatically. In the process, due to the sharp increase of refractive index and strong dispersion of the incident EMW, its wave velocity decreases, even to 0, resulting in the slow light effect [39]. Therefore, it is suitable for application in the field of optical cache devices. The formula for calculating group delay (t_g) and group refractive index (n_g) is as follows, which is used to characterize the slow light effect index [40,41]:

$$t_g = -\frac{d\varphi}{d\omega} \tag{1}$$

$$n_g = \frac{c}{h} \times t_g \tag{2}$$

In the formula, other parameters c, h, ω, φ respectively represent the speed of light in vacuum, the total thickness of the unit structure, the transmission phase, and the angular frequency of EMW. And standing for the intensity of the slow light effect, the greater the n_g of value shows that the EMW group velocity (compound light speed) v_g is smaller. Fig. 5 (a) displays the curve of the transmission phase with frequency, presenting the abrupt phase jump at the three frequency points of 0.35 GHz, 0.65 GHz, and 1.55 GHz, which approximately correspond to the three transmission dips of the MS. In the EIT transmission window, as shown in the shaded part of Fig. 5(b), the group delay values of the simulation groups are all greater than 0, demonstrating an obvious slow light effect. In the first transparent window between 0.34 GHz and 0.68 GHz, the MS reaches a maximum group delay of 6.35 ns at 0.38 GHz, while in the second transparent window, the maximum group delay is 2.39 ns at 1.46 GHz. Similar to the trend of group delay, the group index reaches the maximum at 158.82 and 59.71 at 0.34 GHz and 1.46 GHz in the two transparent windows, respectively. It suggests that waves travel 158.82 or 59.71 times longer in MS than in air of the same thickness,

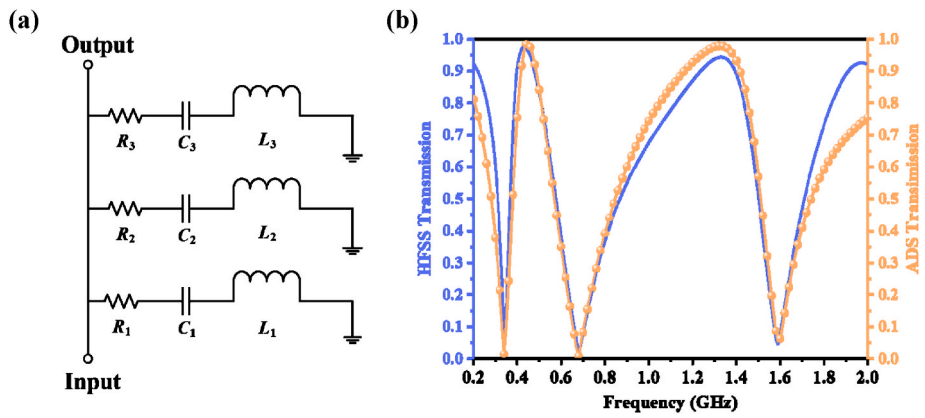

Fig. 6. Equivalent circuit fitting:(a) schematic diagram of equivalent circuit of the proposed EIT MS, and (b) transmission coefficients by HFSS and ADS.

Table 3
The summary of values of circuit elements.

Element	Value	Element	Value	Element	Value
R_1	0.1 Ω	C_1	6.915 pF	L_1	7.955 nH
R_2	0.3 Ω	C_2	9.413 pF	L_2	23.2 nH
R_3	1.3 Ω	C_3	0.891 pF	L_3	11.215 nH

respectively, meaning the proposed EIT MS has unlimited prospects in the slow light realm.

The realization of the EIT effect in MS requires the joint action of two modes. Therefore, there is a discussion about the equivalent circuit under the coupling effect of bright and dark modes of EIT. The composite structure has three resonance points. So if Resistance-Inductance-Capacitance (RLC) resonant circuit is adopted, only three RLC series branches are required to be connected in parallel to fit the EIT effect as displayed in Fig. 6(a). The specific values of the circuit elements have been summarized in Table 3. In Fig. 6(b), it is obvious that at the three transmission valleys and two peaks, the simulation results of HFSS fit well with the equivalent circuit.

To verify the EIT effect of the structure, a fabricated sample as exhibited in Fig. 7(a) has been made and its S parameter of transmission has been tested by a vector network analyzer (VNA). In Fig. 7(b), electromagnetic excitation is applied to the structure by means of two coaxial cables to Sub Miniature version A (SMA) connectors of the VNA for testing purposes. As shown on the display of the VNA, a comparison between the experiment result and simulation data is stated in Fig. 7. For the first transparent window, the fitting between the experiment and simulation is still adjacent, taking the frequency offset of 0.1 GHz between the second transmission valley into account. In terms of the second transparent window, in contrast, with the transmission zero obtained by simulation, the transmission zero measured by the experiment is shifted by 0.26 GHz to the high-frequency direction, which makes the bandwidth of EIT significantly widen. In general, this kind of deviation can be tolerated in the practical application for the reason that the proposed structure still achieves the dual-band broadband EIT phenomenon well within the specified frequency band. The main factors for the difference may include the precision of the manufacturing process, the distinction between the experimental and ideal conditions, and

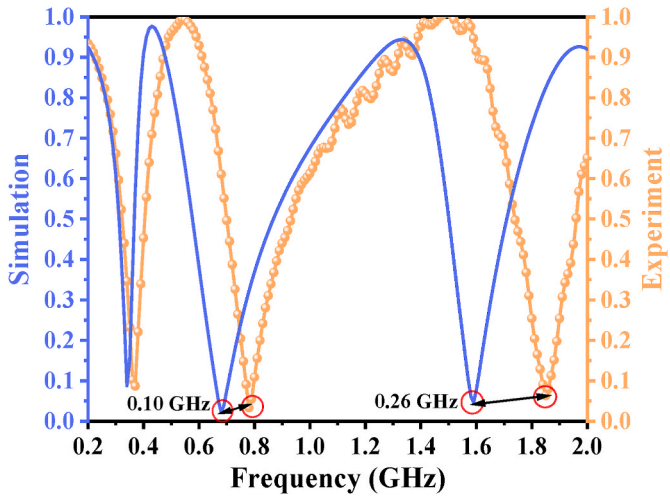

Fig. 8. Simulated and experimented transmission spectra of the proposed MS.

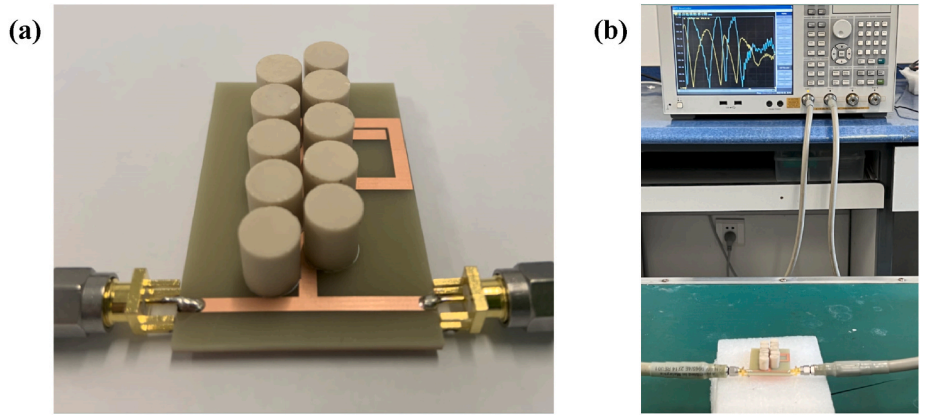

Fig. 7. The photograph of the experiment: (a) the fabricated sample, and (b) connection diagram of sample and VNA.

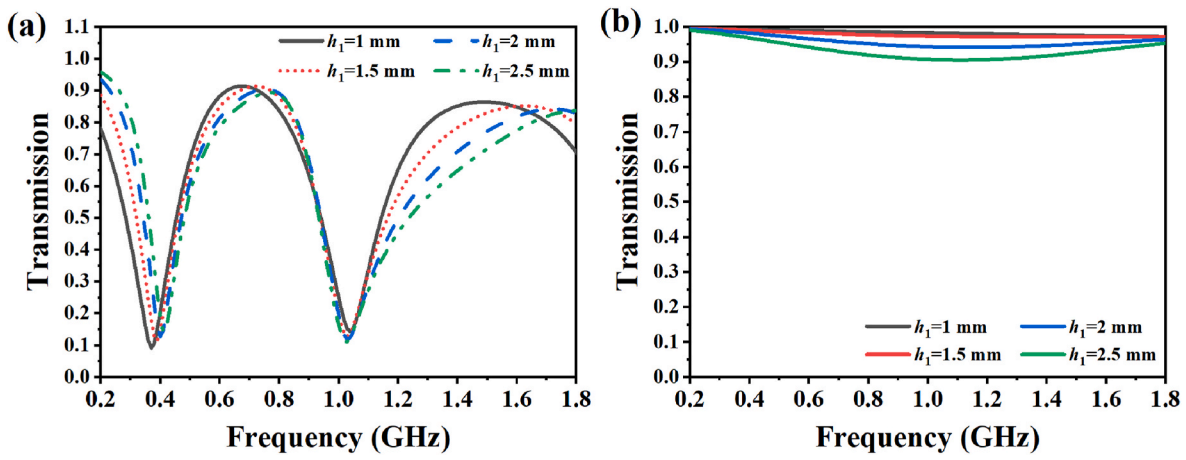

Fig. 9. The effect of h_1 on the proposed MS: (a) the bright mode, (b) the dark mode.

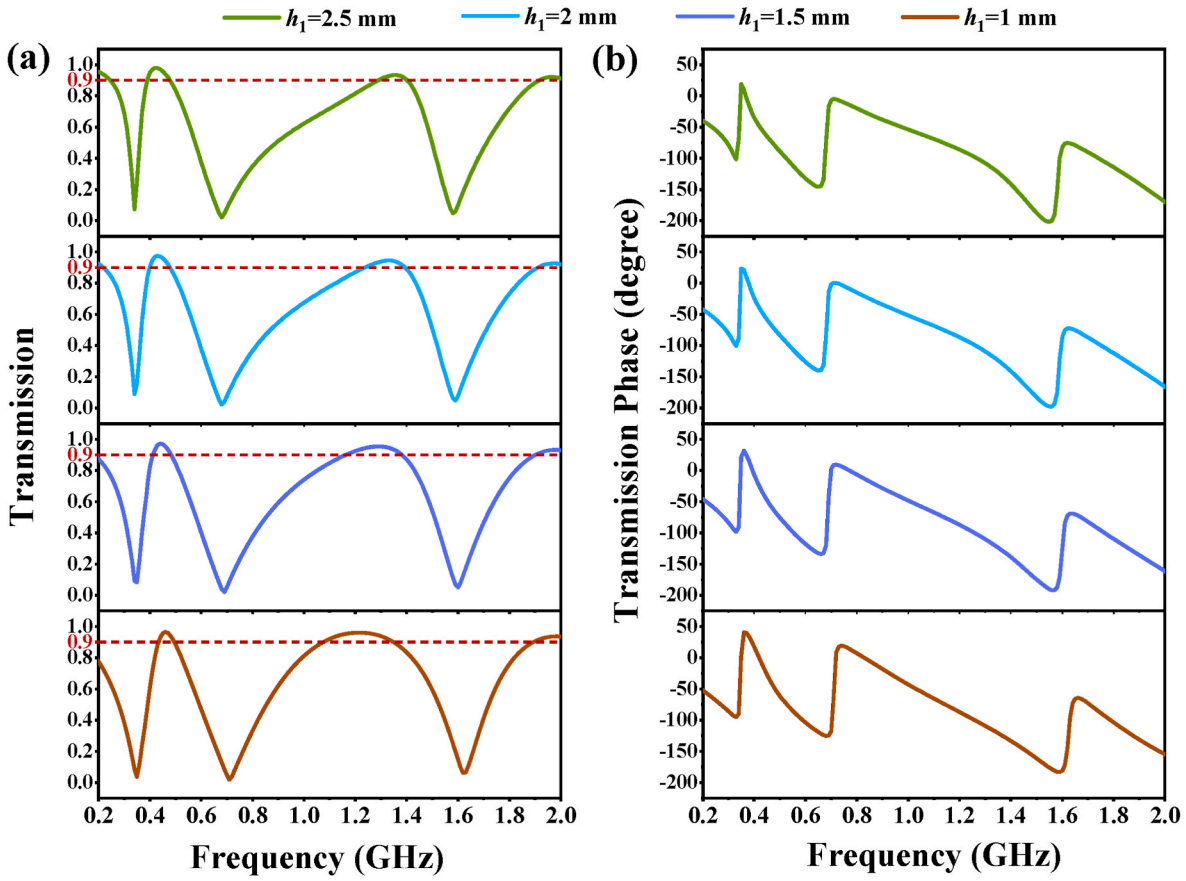

Fig. 10. The influences of h_1 on transmission and transmission phase: (a) transmission, and (b) transmission phase.

the parameters of the production materials which cannot be completely consistent with the simulation (see Fig. 8).

4. Parameter discussion and physical mechanism analysis

The parameter discussion section is mainly divided into MSL structure, CMT structure, and the common part of both. h_1 is the thickness of the dielectric substrate. In this structure, because of the weak response of the dark mode, the adjustment of the EIT phenomenon is mainly achieved by adjusting the resonant response of the bright mode to EMW, which can also be seen in Fig. 9 showing the effect of h_1 on the bright and dark modes respectively. Despite that h_1 has no significant influence on the frequency and value of the two transmission dips of the bright mode, it still has an impact on the frequency of the second transmission peak of the bright mode, demonstrating that with the increase of h_1, the second peak tends to move to high frequency. For the dark mode, the change of h_1 has a weak effect on the resonance in Fig. 9(b), for the reason that when h_1 increases from 1 mm to 2.5 mm, the dark mode transmission rate only decreases by about 0.1. In Fig. 10, taking that h_1 has no obvious effect on the resonant frequency of the bright mode into consideration, the transmission valley generated by the coupling between the bright mode and the dark mode will not shift significantly with the change of h_1 when they are combined. However, the second transmission peak of the bright mode changes, so the transmission of the

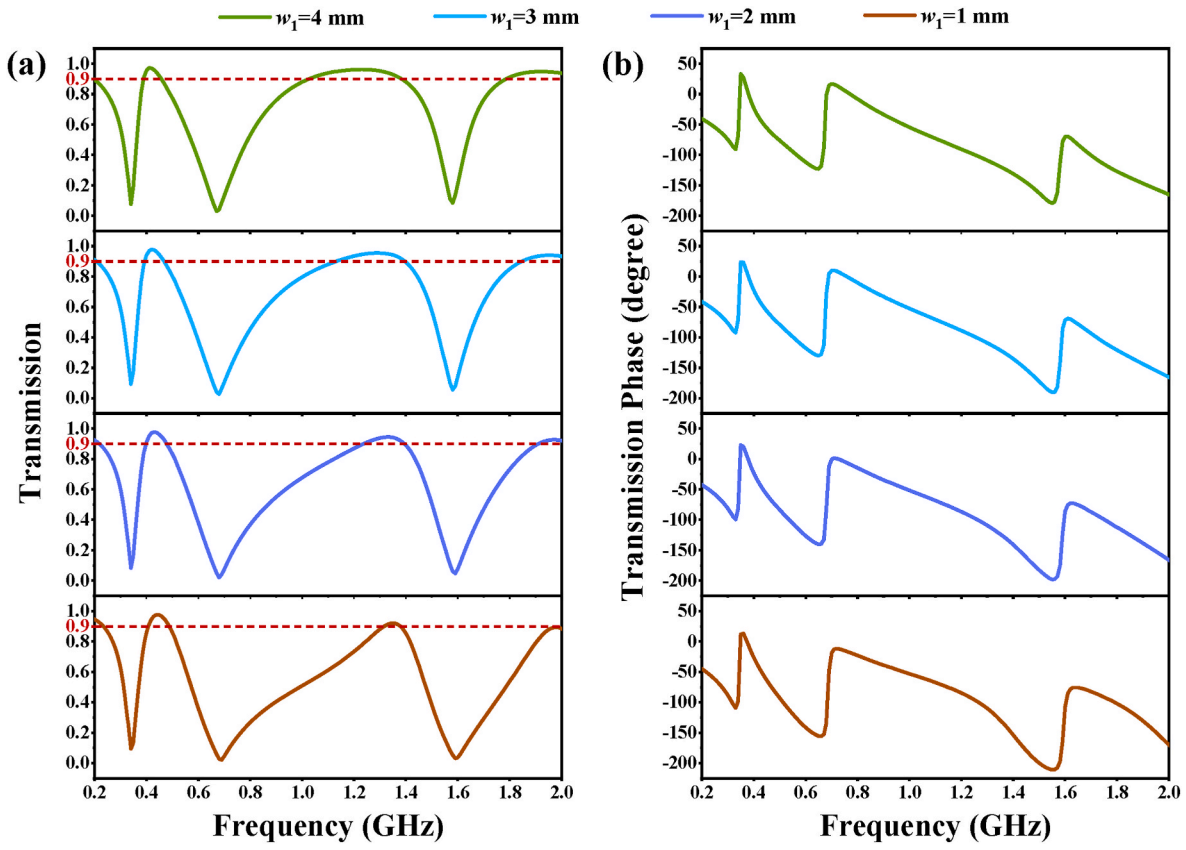

Fig. 11. The influences of w_1 on transmission and transmission phase: (a) transmission, and (b) transmission phase.

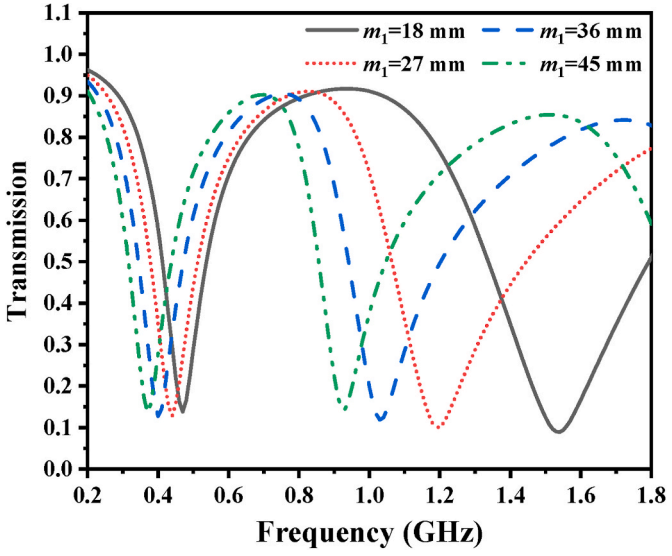

Fig. 12. The effect of m_1 on the bright mode.

second peak of the combined structure shows a decreasing trend, resulting in a significant narrowing of the frequency band with transmittance exceeding 0.9. Correspondingly, the phase change in this frequency band is smoother and faster, with h_1 varying from 2.5 mm to 1 mm.

The influences of FR_4 substrate thickness on the EIT effect and transmission phase are displayed in Fig. 11. The FR_4 dielectric layer has little effect on the position and transmittance of three transmission zero points, thus the two transparent windows of the EIT are almost unaffected. However, the second transmission peak of the bright mode will change, so the transmission of the second transmission peak of the combined structure shows a decreasing trend, resulting in a significant narrowing of the frequency band with transmittance exceeding 0.9. Correspondingly, the phase change in this frequency band is smoother and faster, with h_1 varying from 2.5 mm to 1 mm. On the sharp contrary, the linear width w_1 of the transverse MSL on the dielectric substrate embodies a distinct effect on the transmittance of the MS as displayed in Fig. 11. The augment of w_1 can bring about the increase of the transmission of the structure. But the larger w_1, the wider part whose transmission peak exceeds 90%. Frequency bands with faster transmittance change are also accompanied by faster phase change as shown in Figs. 10(b) and Fig. 11(b).

In terms of the bright mode structure, it can be divided into two parts, namely the spiral wire patch and the MSL. m_1 is used in the proposed structure to represent the length of a quarter branch line of the MSL. Therefore, to discuss the influence of m_1 on the EIT phenomenon of the composite structure, it is actually to analyze the effect of m_1 on the electromagnetic response of the bright mode. The influence of m_1 on the bright mode is mainly manifested in the frequency offset of the resonant point, displayed in Fig. 12 m_1 increasing, both resonant points of bright mode will move to the low-frequency direction. The larger m_1 will bring a greater distance between the overall spiral wire structure and the transverse patch. Therefore, under the combined MS, the increase of m_1 will significantly affect the two transparent windows of EIT, while the impact on the transmittance is slight. The first transmission valley is almost unaffected by m_1. However, with the increase of m_1, the second and third transmission zeros will move to the low-frequency direction, which results in the formation of a dual-band EIT phenomenon within 0.2 GHz~2 GHz. This is mainly because the generation of EIT is due to the interference effect between the bright mode and the dark mode, so a new transmission peak is generated in the originally opaque frequency band, and a new transmission dip is also formed (see Fig. 13).

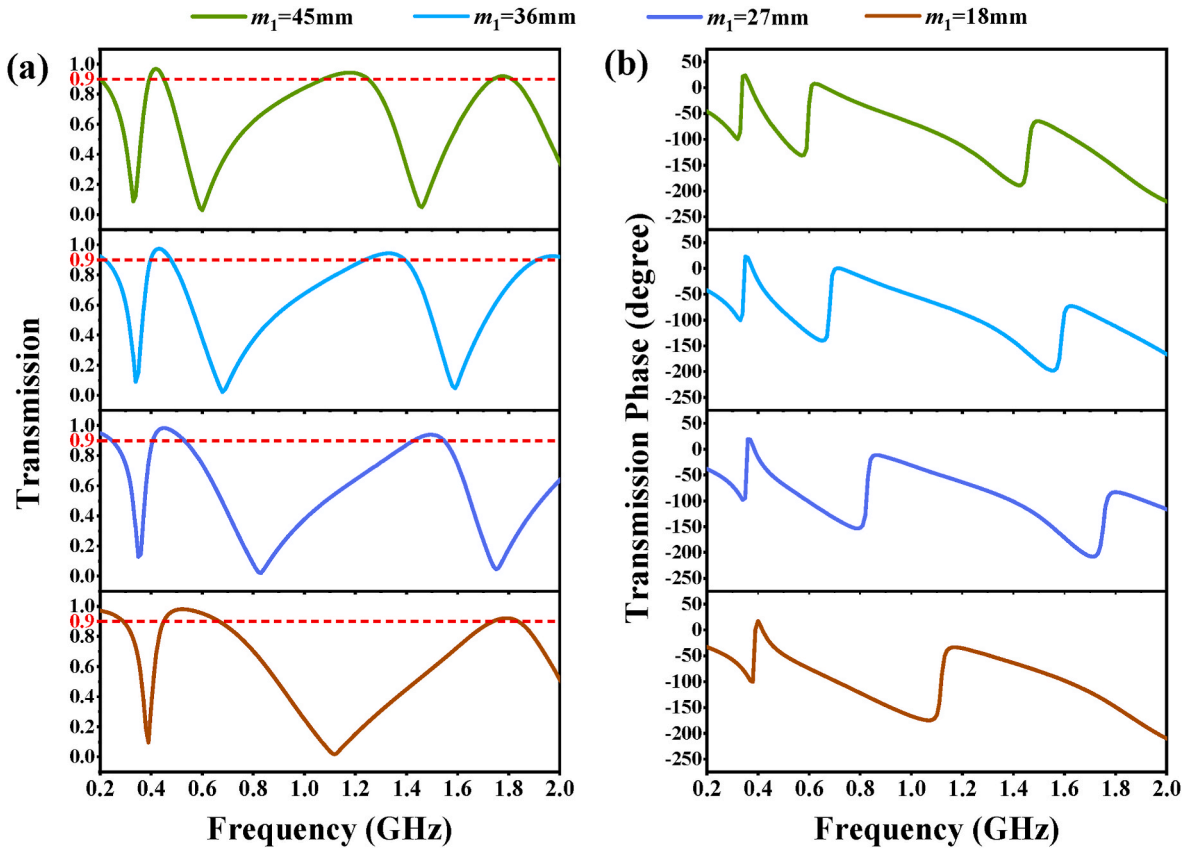

Fig. 13. The influences of m_1 on transmission and transmission phase: (a) transmission, and (b) transmission phase.

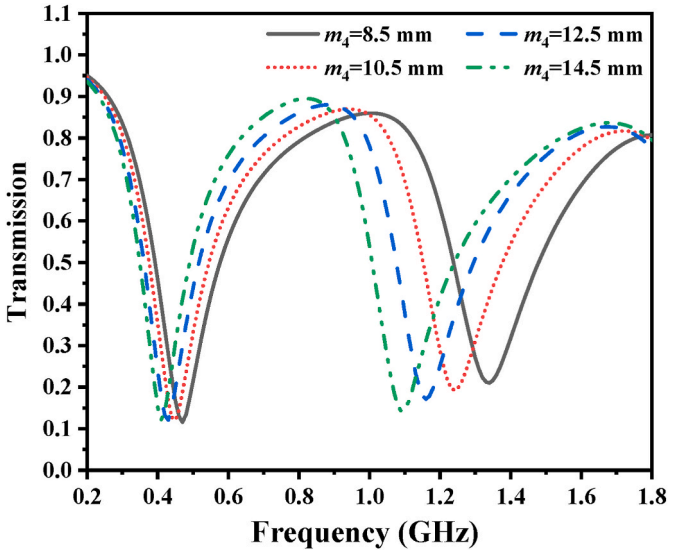

Fig. 14. The effect of m_4 on the bright mode.

m_4 is the inner circle width of the spiral, which is also a structure only found in the bright mode. Fig. 14 displays how m_4 exerts influence on the bright mode. The effect of m_4 on the first resonant point of the bright mode is very tiny and almost negligible. When m_4 is 14.5 mm and m_4 is 8.5 mm, the frequency offset in both cases is only 0.1 GHz, and the transmittance is almost unchanged. The main function of m_4 is reflected in the change of the second resonant point. Not only will the increase of m_4 cause the resonant point to move to the low-frequency direction but also reduce the transmission rate. With this change, the transmission peak will also shift. Based on this, when the bright and dark modes work together, Fig. 15 shows the influence of m_4 on the EIT effect. Except for m_1 and m_4, m_5 also affects the size of the inner circle of the spiral wire, thus influencing the EIT effect.

As for the impact of m_5, which is displayed in Fig. 16, it plays a obvious role in the EIT effect, whose addition will bring two EIT bands to the lower frequency. When m_5 is less than 12 mm and decreases from 11.5 mm to 4 mm, the second EIT window will widen and move towards the high frequency. The phase jump points correspond to the transmittance trough of the MS and also shift to high frequency with the resonant frequency point. Noting when m_5 is equal to 12 mm, the EIT effect of the MS transforms greatly, manifesting that there are only two resonance points in 0.2 GHz~2 GHz, that is to say, only single-band EIT can be realized. The main reason for this phenomenon is that at this time, the spiral structure of the inner ring and the outer ring contact, becoming into a sealed square ring, so the resonance has also changed significantly.

In the dark mode of the structure, the CMT ceramic cylinders are crucial components. Targeted at a further discussion about the influence of ceramic materials on the EIT effect in the structure, the transmission curves of a variety of CMT ceramic cylinders distribution are simulated. It is shown in Fig. 17 that ceramic cylinders have a momentous and apparent influence on bandwidth and transmission peaks. In Fig. 17(a)–(d), there are five CMT cylinders in the dark mode, with different distributions. According to Fig. 17(a) and (d), the cylinders and spiral structure are closer to each other, so the coupling is stronger. As a result, the structure still presents a dual-band broadband EIT effect. In Fig. 17 (b) and (c), the second transparent window tends to shift back or even disappear. Moreover, it is obvious that the cylindrical distribution in Fig. 17(g) and (f) will cause the third transmission zero to move towards the high frequency, which may lead to the widening of the transparent window of the structure. In the case shown in Fig. 17(h) and (i), the MS

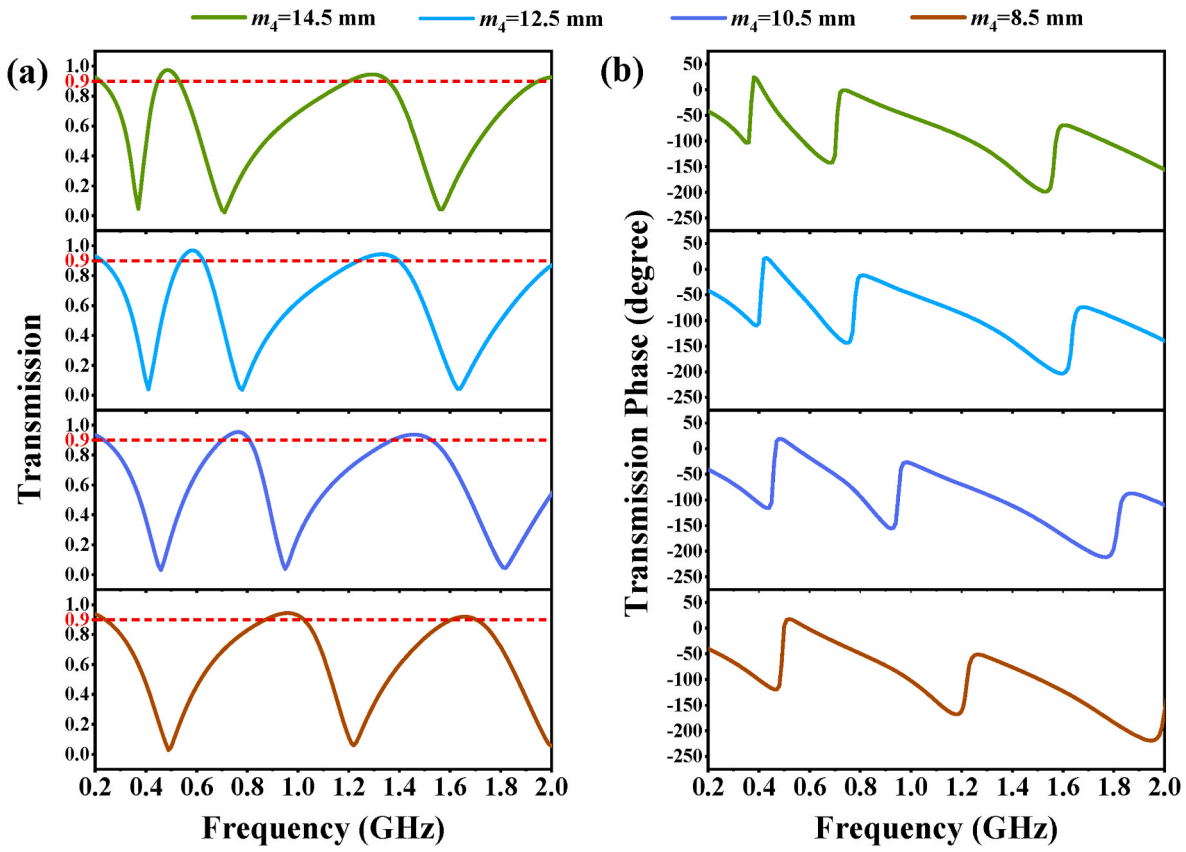

Fig. 15. The influences of m_4 on transmission and transmission phase: (a) transmission, and (b) transmission phase.

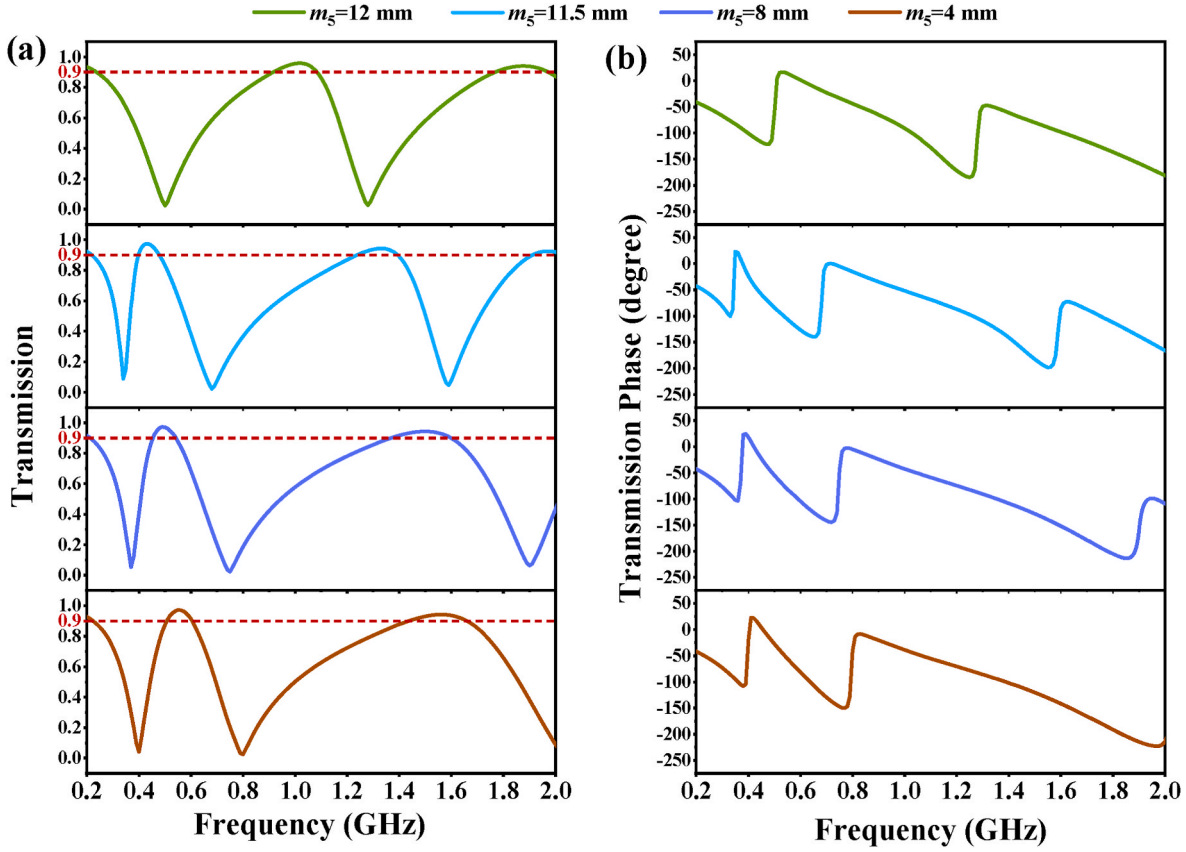

Fig. 16. The influences of m_5 on transmission and transmission phase: (a) transmission, and (b) transmission phase.

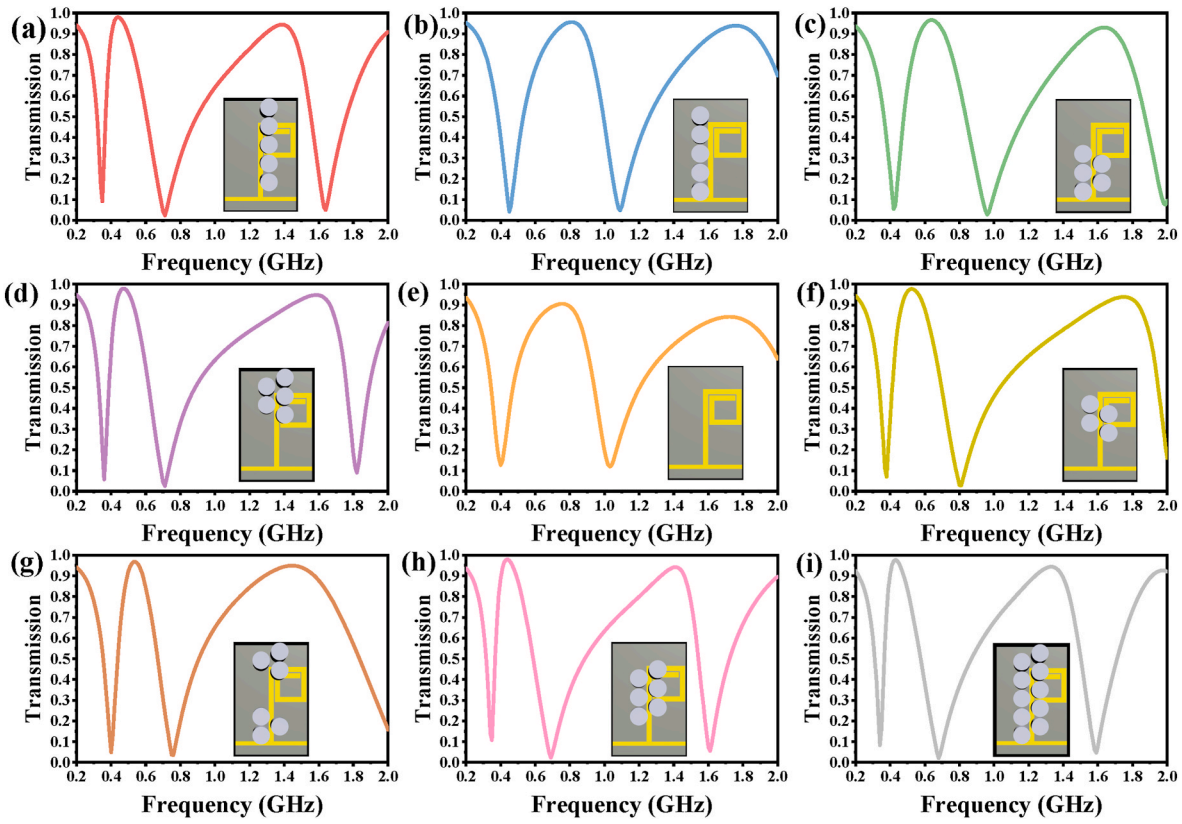

Fig. 17. The transmission spectra corresponding to the different CMT cylinders distribution.

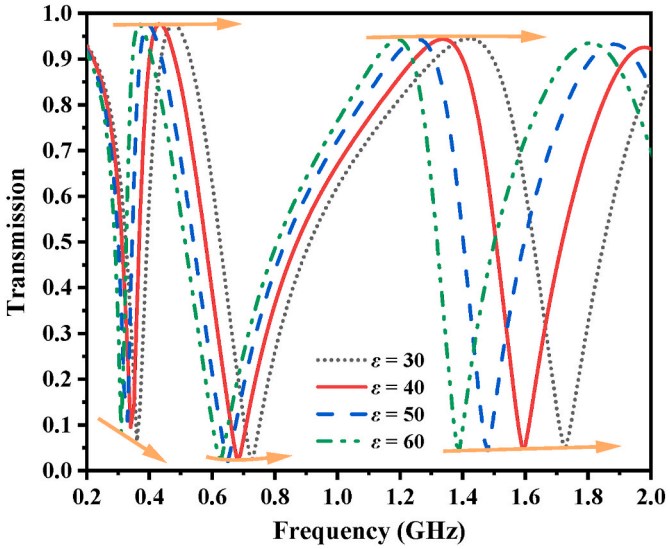

Fig. 18. The transmission spectra of ceramic cylinders with different ceramic constants ε.

will produce two EIT windows within 0.2 GHz~2 GHz, in which case the CMT cylinders and spiral wires are coupled strongly. Through the discussion of these cases, it is not difficult to draw the conclusion that when the position of the ceramic cylinders and the spiral wires are close, that is, when the coupling is strong, the MS will generate two broadband EIT transparent windows at a lower frequency. On the contrary, when the distance between the CMT ceramic cylinders and the spiral wires is huge, the EIT phenomenon tends to move toward high frequency. Therefore, we can arrange the CMT ceramic cylinders flexibly according to this circumstance.

In addition to the arrangement of the CMT cylinders, the dielectric constant ε of the ceramic dielectric material used in the cylinders is also one of the parameters that should be considered which may affect the EIT effect. Fig. 18 displays the impact of ε on EIT. Obviously, the dielectric constant ε of the cylinder has an obvious effect on the position of the resonant frequency point, while the effect on the value of the transmittance is negligible. The dielectric constant ε increases from 30 to 60, giving rise to the result that the EIT window also moves to the low-frequency direction. According to the required working frequency position, it is reasonable to select the ceramic dielectric cylinders with the appropriate dielectric constant ε.

The electric field analysis of the structure is carried out according to the coupling theory of bright mode and dark mode. Fig. 19 depicts the electric field on the upper surface of bright and dark modes at 0.4 GHz and 1.03 GHz. Analyzing the electric field distribution, it is reasonable to define the two structures as bright mode and dark mode respectively, for the reason that the bright mode resonates strongly with EMW, while the dark mode resonates slightly. The bright mode has resonance points at 0.3 GHz and 1.03 GHz respectively, whose electric field distribution is reflected in Fig. 19(a) and (b). At these two resonant points, the bright mode and EMW will generate resonance, thus forming a transmission valley, so the electric field at the two frequency points is relatively strong. Nonetheless, the structure is different from the resonance of EMW. At 0.4 GHz, the electric field of bright mode is mainly concentrated in the inner ring of the spiral structure, which can be inferred that the transmission dip mainly originated from the resonance between EMW and spiral resonance. As can be seen from Fig. 19(b), the spiral structure is coupled with the MSL, leading to the phenomenon that the electric field is mainly concentrated on the two, thus forming a resonance point at 1.03 GHz.

However, at these two resonant points of the bright mode, the response of the dark mode to the EMW is weaker, which can also be seen

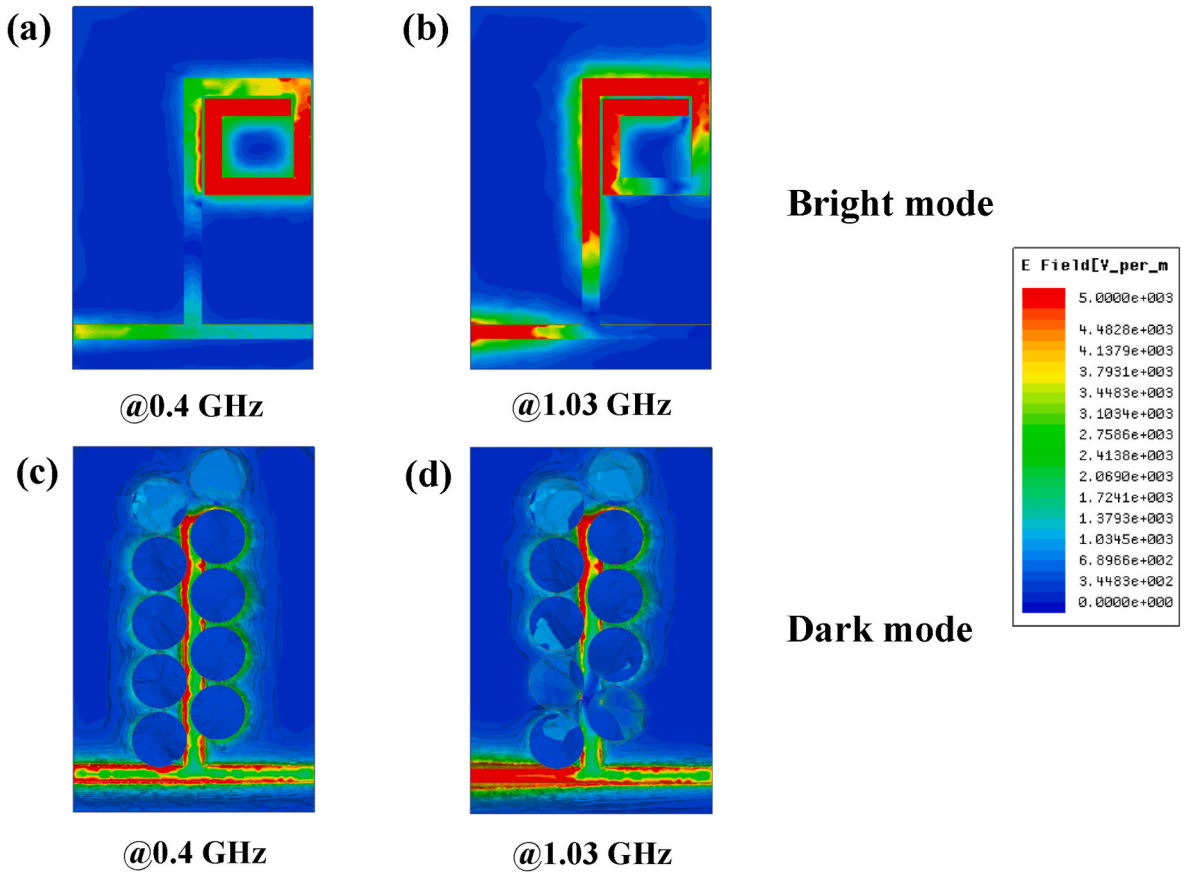

Fig. 19. Electric field distribution on the upper surface of different structures: (a) bright mode at 0.4 GHz, (b) bright mode at 1.03 GHz, (c) dark mode at 0.4 GHz, and (d) dark mode at 1.03 GHz.

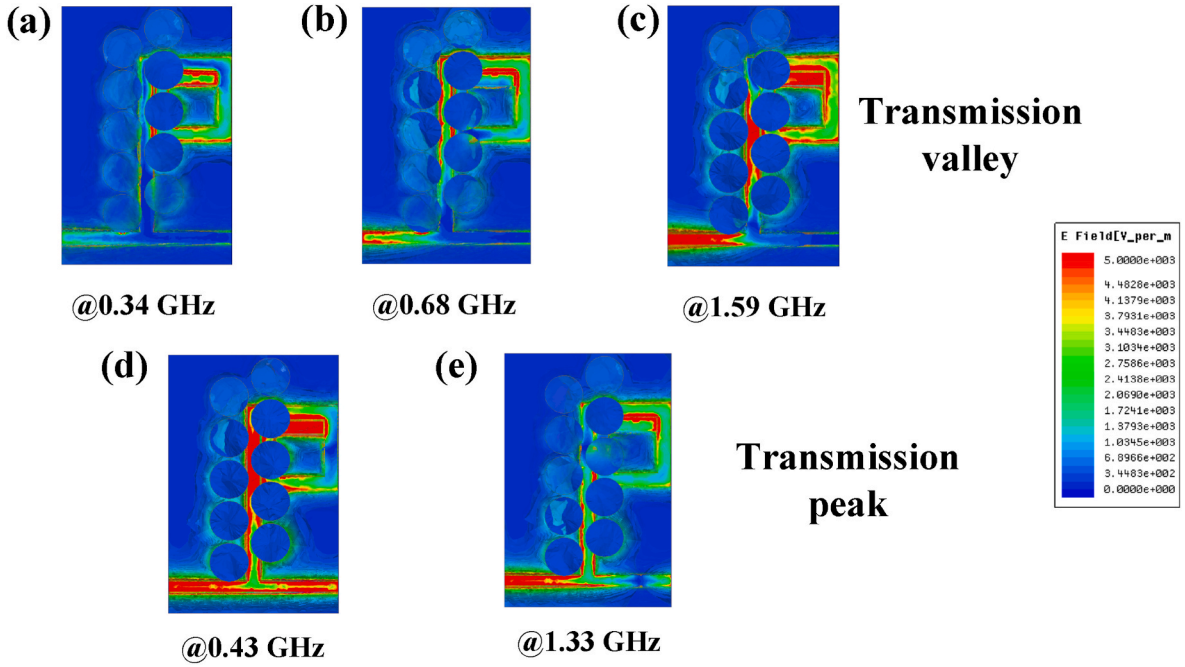

Fig. 20. Electric field distribution on the upper surface of complete structures at different frequency: (a) at 0.34 GHz, (b) at 0.68 GHz, (c) at 1.59 GHz, (d) at 0.43 GHz and (e) 1.33 GHz.

in Fig. 4(a). Therefore, the electric field distribution of the two points is similar, only the electric field is stronger at the edge of the MSL, which indicates that the structure is not strongly coupled to EMW at this time, which is why no obvious transmission valley is formed when the dark mode acts alone.

When the bright mode and the dark mode work together, they will be coupled with each other, resulting in destructive interference, which makes the original opaque place produce a new resonance point and obtain a new transparent window, which phenomenon is called EIT. Fig. 20 respectively fits the electric field distribution at three transmission valleys and two transmission peaks. Fig. 20(a)–(c) are transmission valleys and (d)-(e) are transmission peaks. From the three electric field distributions corresponding to the transmission valleys, it can be seen that there is also a partial electric field distribution at the bottom of the CMT ceramic dielectric cylinder, which means that the coupling between the bright mode and the dark mode also occurs. At the transmission peak, the electric field is mainly concentrated on the MSL structure and the spiral structure.

5. Conclusion

In this paper, by combining the MSL structure with CMT ceramic structure, the dual-band EIT is realized from the new design. The proposed EIT MS has realized the dual-band EIT effect in 0.2 GHz~1.6 GHz. The feasibility and rationality of the structure are verified by circuit fitting and experimental measurement. The designed sample is verified by experiments, offering the convinces to confirm the validity and feasibility of the dual-band EIT effect. In addition, the influence of CMT ceramic structure as a dark mode on the EIT effect in structural modification is discussed in depth. By discussing the key parameters of the structure and simulating the surface current, the physical mechanism of the structure is discussed deeply. What is more, the EIT MS has been proven to possess an obvious slow light effect, making it have tremendous potential application value in slow light device fabrication.

CRediT authorship contribution statement

Haining Ye: Data curation, Formal analysis, Investigation, Writing – original draft, Visualization. **Baofei Wan:** Software, Validation. **Hanqing Dong:** Software, Validation. **Haifeng Zhang:** Conceptualization, Methodology, Supervision, Writing – review & editing.

Declaration of competing interest

The authors declare that they have no known competing financial interests or personal relationships that could have appeared to influence the work reported in this paper.

References

[1] L. Wang, Z. Gao, Z. Hou, J. Song, Y. Shi, Active modulation of an all-dielectric metasurface analogue of electromagnetically induced transparency in terahertz, ACS Omega 6 (2021) 4480–4484.

[2] Z. Lei, F. Meng, D. Liang, Q. Wu, B. Che, G. Ju, J. Fu, Z. Kuang, G. Yang, Magnetic metamaterial analog of electromagnetically induced transparency and absorption, J. Appl. Phys. 117 (2015), 063901.

[3] N. Liu, T. Weiss, M. Mesch, L. Langguth, U. Eigenthaler, M. Hirscher, C. Sonnichsen, H. Giessen, Planar metamaterial analogue of electromagnetically induced transparency for plasmonic sensing, Nano Lett. 10 (2010) 1103–1107.

[4] H. Li, F. Xue, Tailoring polarization of electromagnetically induced transparency based on non-centrosymmetric metasurfaces, Phys. Lett. 11 (2017) 1–5.

[5] K.J. Boller, A. Imamolu, S.E. Harris, Observation of electromagnetically induced transparency, American Physical Society 66 (1991) 2593–2596.

[6] J. Dhanya, A.V. Basiluddeen, R. Ratheesh, Synthesis of ultra low temperature sinterable $Na_2Zn_5(MoO_4)_6$ ceramics and the effect of microstructure on microwave dielectric properties, Scripta Mater. 132 (2017) 1–4.

[7] P. Palinginis, F. Sedgwick, S. Crankshaw, M. Moewe, C. Chang-Hasnain, Room temperature slow light in a quantum-well waveguide via coherent population oscillation, Opt Express 13 (2005) 9909–9915.

[8] X. Yang, M. Yu, D.L. Kwong, C.W. Wong, Coupled resonances in multiple silicon photonic crystal cavities in all-optical solid-state analogy to electromagnetically induced transparency, IEEE J. Sel. Top. Quant. 16 (2010) 288–294.

[9] J. Jose, H. Wanare, Bio-organism detection in one-dimensional photonic crystals using electromagnetically induced transparency, Opt. Lett. 37 (2012) 410.

[10] A. Naweed, Evolution of all-optical electromagnetically induced absorption and transparency in triple-microcavity-based one-dimensional photonic crystals, OSA Continuum 4 (2021).

[11] C. Dong, T. Wang, Y. Jin, X. Li, B. Wang, J. Tang, All-optical analog to electromagnetically induced transparency effects for multiple wavelengths in a silicon photonic crystal coupled cavity system, Opt Commun. 315 (2014) 26–31.

[12] S. Liu, J. Dong, J. Si, W. Yang, X. Yu, J. Zhang, X. Deng, Bidirectional electromagnetically induced transparency based on coupling of magnetic dipole modes in amorphous silicon metasurface, Nanomaterials (2021) 6.

[13] Y. Zhao, W. Bian, B. Huang, Q. Cheng, Switchable broadband terahertz absorber/reflector enabled by hybrid graphene-gold metasurface, Opt Express 25 (2017) 7161–7169.

[14] B. Han, X. Li, C. Sui, J. Diao, X. Jing, H. Zhi, Analog of electromagnetically induced transparency in an E-shaped all-dielectric metasurface based on toroidal dipolar response, Opt. Mater. Express 8 (2018) 2197–2207.

[15] T. Zang, Y. Chen, Y. Ding, Y. Sun, Q. Wu, Broadband electromagnetically induced transparency in metamaterials based on hybridization bandgap, AIP Adv. 10 (2020), 115002.

[16] X. Shi, Y. Tong, Y. Ding, Polarization-independent and angle-insensitive tunable electromagnetically induced transparency in terahertz metamaterials, Appl. Opt. 60 (2021) 7784–7789.

[17] Y. Xu, X. Wang, X. Chen, L. Zhang, Structure-based tunable metamaterials for electromagnetically induced transparency windows in low terahertz frequency, J. Appl. Phys. 127 (2020), 034501.

[18] G. Li, F. Yan, W. Wang, N. Qiao, Analysis of multiband and broadband electromagnetically induced transparency based on three-dimensional coupling, Laser & Optoelectron 55 (2018), 121601.

[19] S. Hu, H. Yang, H. Song, X. Huang, B. Xiao, Tailoring dual-band electromagnetically induced transparency in planar metamaterials, J. Appl. Phys. 117 (2015) 4773.

[20] Y. Jiang, X. Zhu, Z. Song, Achieving dual-band absorption and electromagnetically induced transparency in VO2 metamaterials, Phys. Bull. 624 (2022), 413391.

[21] L. Zhu, F. Meng, J. Fu, Q. Wu, J. Hua, Multi-band slow light metamaterial, Opt Express 20 (2012) 4494–4502.

[22] R. Ning, Z. Jiao, J. Bao, Multi-band and wide-band electromagnetically induced transparency in graphene metasurface of composite structure, IET Microw., Antennas Propag. 12 (2018) 380–384.

[23] H. Iizuka, T. Watanabe, K. Nishikawa, Millimeter-wave microstrip line to waveguide transition fabricated on a single layer dielectric substrate, IEICE Trans. Commun. 85 (2002) 1169–1177.

[24] J. Wang, X. Tian, J. Jiang, Z. Geng, Dual-spectral plasmon electromagnetically induced transparency in planar metamaterials based on bright–dark coupling, Opt Commun. 291 (2013) 371–375.

[25] Z. Xu, S. Liu, S. Li, X. Yin, Analog of electromagnetically induced transparency based on magnetic plasmonic artificial molecules with symmetric and antisymmetric states, Phys. Rev. B 99 (2019), 041104, 1-041104.5.

[26] L. Zhu, J. Fu, F. Meng, X. Ding, L. Dong, Q. Wu, Detuned magnetic dipoles induced transparency in microstrip line for sensing, IEEE Trans. Magn. 50 (2014) 1–4.

[27] J. Tao, J. Jiang, S. Zhao, Y. Zhang, X. Li, X. Fang, P. Wang, W. Hu, Y. Lee, H. Lu, D. Zhang, Fabrication of 1D Te/2D ReS2 MixedDimensional van der Waals p-n heterojunction for high-performance phototransistor, ACS Nano 15 (2021) 3241.

[28] J. Tao, H. Ma, K. Yuan, Y. Gu, J. Lian, X. Li, W. Huang, M. Nolan, H. Lu, D. Zhang, Modification of 1D TiO2 nanowires with GaOxNy by atomic layer deposition for TiO2@GaOxNy core-shell nanowires with enhanced photoelectrochemical performance, Nanoscale 12 (2020) 7159.

[29] Y. Wu, Z. Dong, Y. Chen, B. Wang, L. Wang, X. Dai, J. Zhang, X. Wang, Optimization of pixel size and electrode structure for Ge:Ga terahertz photoconductive detectors, Sensors 22 (2022) 1916.

[30] Y. Chen, Z. Dong, Y. Zhou, J. Tao, W. Tong, Y. Wu, W. Liu, B. Wang, X. Dai, X. Wang, Wavelength modulation characteristics of metal gratings on Si-based blocked-impurity-band (BIB) terahertz detectors, Micromachines 13 (2022) 811.

[31] Q. Yuan, H. Jiang, J. Wang, J. Wang, J. Zhang, Q. Lei, B. Shao, Stable permittivity and low loss Al2O3 ceramic based metasurface achieves broadband polarization conversion at high temperature, Ceram. Int. 47 (2021) 7268–7271.

[32] Z. Dong, Y. Zhou, Y. Chen, J. Tao, W. Liu, X. Dai, B. Wang, Y. Wu, X. Wang, The anti-reflection coating design for the very-long-wave infrared Si-based blocked impurity band detectors, Crystals 13 (2023) 60.

[33] J. Wu, J. Tao, C. Zhang, H. Zhang, L. Zhang, D. Chen, X. Wang, The high-performance linear scan imaging system of terahertz Si-based blocked-impurity-band detector, Frontiers in Electronic Materials 2 (2023), 1107802.

[34] B. Wang, Y. Chen, W. Tong, Y. Zhou, J. Tao, Z. Wang, Z. Dong, H. Zhou, Z. Fu, D. Shao, X. Wang, J. Cao, Spectral modulation of blocked-impurity-band hybrid structure terahertz detector, Appl. Phys. Lett. 120 (2023), 071102.

[35] X. Wang, W. Ma, Y. Chen, X. Chen, B. Wang, C. Zhang, H. Zhang, Spectral response mechanism associated with the thickness of the absorbing layer in GaAs-based blocked-impurity-band (BIB) far-infrared detectors, Opt. Quant. Electron. 53 (2021) 326.

[36] P. Munaga, S. Ghosh, S. Bhattacharyya, K.V. Srivastava, A fractal-based compact broadband polarization insensitive metamaterial absorber using lumped resistors, Microw. Opt. Technol. Lett. 58 (2015) 343–347.

[37] H. Dai, Y. Zhao, J. Chen, C. Yu, L. Xing, Ultra-wideband radar cross-section reduction using polarization conversion metasurface, Int. J. RF Microw. C. E. 30 (2020) 1–6.
[38] N. Xu, M. Manjappa, R. Singh, W. Zhang, Tailoring the electromagnetically induced transparency and absorbance in coupled fano–lorentzian metasurfaces: a classical analog of a four-level tripod quantum system, Adv. Opt. Mater. 4 (2016).
[39] Y. Ye, J. Shen, Y. Jin, Manipulating light flow with one-dimensional photonic crystals of an electromagnetically induced transparency medium, Appl. Phys. A Mater. Sci. Processing 93 (2008) 505–509.
[40] S.Y. Chiam, R. Singh, C. Rockstuhl, F. Lederer, W. Zhang, A.A. Bettiol, Analogue of electromagnetically induced transparency in a terahertz metamaterial, Phys. Rev. B 80 (2009), 153103.
[41] C. Sui, B. Han, T. Lang, X. Li, X. Jing, H. Zhi, Electromagnetically induced transparency in an all-dielectric metamaterial-waveguide with large group index, IEEE Photon. J. 9 (2017) 1–8.